REMARKS

Interview

Applicants would like to thank Examiner Layla Soroush and Supervisory Examiner Sreeni Padmanabhan for the phone interview held with Applicants' representative on April 14, 2010. During the phone interview, Applicants' representative proposed arguments for overcoming the rejections. Examiner Layla Soroush and Supervisory Examiner Sreeni Padmanabhan agreed to consider the arguments when submitted in writing. Applicants have incorporated the proposed arguments in the response below.

Status of the Claims

Claims 33, 53-57, 61, 62, 64, 66, 68, 70-73, and 75-83 are currently pending. Claim 1-32, 34-52, 58-60, 63, 65, 67, and 69 have been canceled without prejudice or disclaimer of the subject matter claimed therein. Claims 33, 53-57, 61, 62, 64, 66, 68, 70-74, and 78 are withdrawn from consideration as being directed to a non-elected invention. New claim 83 is directed to the same invention as claims 75-77 and 79-82. Claims 75-77 and 79-83 are under examination.

Claims 75, 76, and 77 have been amended. Representative support for the amendments to claims 75, 76, and 77 can be found in original claims 58, 59, and 60.

New claim 83 has been added. Representative support for new claim 83 can be found in original claim 65.

Rejection Under 102(b)

Claims 58, 60, 63, 65, 67, and 69 are rejeeted under 35 U.S.C. 102(b) as being anticipated by WO 96/04017 (Kresse, English Equivalent U.S. Patent 6,048,515).

Without acquiescing to the propriety of the rejection, claims 58, 60, 63, 65, 67, and 69 have been canceled. Accordingly, Applicants request withdrawal of the rejection.

Rejection Under 35 U.S.C. § 103(a)

Claims 59, 74-77, and 79-82 are rejected under 35 U.S.C. § 103(a) as allegedly being

obvious over Kresse, as applied to claims 58, 60, 63, 65, 67, and 69 above, and further in view of Boehm (Boehm *et al.*, J. Pharm. Belg. 55: 40-48, 2000).

Kresse does not disclose the claimed invention because Kresse fails to teach each of the steps of the claimed method. As acknowledged on page 5 of the Office Action, Kresse does not teach measuring the zeta potential or measuring the isoelectric point of a composition comprising an active agent and one or more cationic components. Moreover, Kresse does not teach selecting a composition having a zeta potential in the range of about +30 mV to +65 mV in about 0.05 mM KCl solution at about pH 7.5 or selecting a composition having an isoelectric point above 7.5. Applicants respectfully point out that the inventors surprisingly found that compositions having a zeta potential in the range of about +30 mV to +65 mV in about 0.05 mM KCl solution at about pH 7.5 or having an isoelectric point above 7.5 effectively target activated vascular sites. Accordingly, the presently claimed method includes the steps of measuring the zeta potential or isoelectric point of the compositions and selecting for compositions having a zeta potential in the range of about +30 mV to +65 mV in about 0.05 mM KCl solution at about pH 7 or having an isoelectric point above 7.5. These steps are not taught by Kresse.

Further, Applicants respectfully point out that Kresse's compositions comprising carboxydextran coated iron oxide particles have a negative zeta potential as evidenced by the attached Thode reference (Thode *et al.*, J. of Pharmaceutical Sciences, 2000, 89 (10): 1317). The Examples of Kresse disclose coating iron oxide with carboxydextran. Figures 7 and 8 of Thode show that various batches of carboxydextran coated iron oxide particles have negative zeta potential. Thus, Kresse's compositions do not fall within the range recited in the claims.

Boehm does not overcome the deficiencies of Kresse because Boehm does not disclose or suggest each of the features that are missing from Kresse. The Office Action alleges that Boehm teaches determining the zeta potential of colloidal drug carrier. However, Boehm does not teach selecting for compositions having a zeta potential in the range of about +30 mV to +65 mV in about 0.05 mM KCl solution at about pH 7 or having an isoelectric point above 7.5. Rather, Boehm teaches that positively charged compositions are unstable because over time at 25 °C, these positively charged compositions have an increased size (see sentence bridging pages 22 and 23, and Tables I). Boehm seems to suggest that associating an active agent with cationic components may result in an unstable composition, while associating an active agent with

anionic components may result in a more stable composition. Accordingly, Boehm teaches away from associating an active agent with cationic components and from selecting for compositions having a positive zeta potential or an isoelectric point above 7.5.

In summary, the inventors unexpectedly discovered that compositions having a zeta potential in the range of about +30 mV to +65 mV in about 0.05 mM KCl solution at about pH 7 or having an isoelectric point above 7.5 have an enhanced efficacy for targeting activated vascular sites. The claims are directed to methods of obtaining such compositions which includes the steps of measuring the zeta potential or isoelectric point of the compositions and selecting for compositions having the recited zeta potential or isoelectric point. The compositions of Kresse do not have a zeta potential within the range of about +30 mV to +65 mV in about 0.05 mM KCl solution at about pH 7 and do not have an isoelectric point above 7.5.

Conclusion

The foregoing amendments and remarks are being made to place the application in condition for allowance. Applicants respectfully request entry of the amendments, reconsideration, and the timely allowance of the pending claims. A favorable action is awaited. Should the Examiner find that an interview would be helpful to further prosecution of this application, she is invited to telephone the undersigned at her convenience.

If there are any additional fees due in connection with the filing of this response, please charge the fees to our Deposit Account No. 50-0310. If a fee is required for an extension of time under 37 C.F.R. §1.136 not accounted for above, such an extension is requested and the fee should also be charged to our Deposit Account.

Respectfully submitted,
Morgan, Lewis & Bockius LLP

/Sally Teng/

Sally P. Teng
Registration No. 45,397

Dated: April 20, 2010
Morgan, Lewis & Bockius LLP
Customer No. **09629**
1111 Pennsylvania Avenue, N.W.
Washington, D.C. 20004
202-739-3000

Two-Time Window and Multiangle Photon Correlation Spectroscopy Size and Zeta Potential Analysis — Highly Sensitive Rapid Assay for Dispersion Stability

KAI THODE,[1, 2] RAINER H. MÜLLER,[2] MAYK KRESSE[1]

[1]Institut für Diagnostikforschung GmbH (IDF) an der Freien Universitat Berlin, Spandauer Damm 130, D-14050 Berlin, Germany

[2]Institut für Pharmazeutische Technologie, Biopharmazie & Biotechnologie, Freie Universität Berlin, Kelchstraße 31, D-12169 Berlin, Germany

Received 12 June 1999; revised 6 June 2000; accepted 27 June 2000

ABSTRACT: Polysaccharide-stabilized iron oxide particles are highly potent contrast agents in magnetic resonance imaging. After intravenous injection, the size of these small or ultrasmall particles strongly influences their distribution in the body. Knowledge about the uniformity of particle size distribution within this particle size range is not accessible by laser diffraction (lower edge of detection range), and photon correlation spectroscopy (PCS) data only yield insufficient information, the so-called polydispersity index. A combination of two-time window and multiangle analysis makes detailed characterization of particle size distribution and particle aggregation feasible, which was shown using five different iron oxide dispersions. Additional particle charge characterization yielded conclusions about the type of stabilization present in the dispersion — electrostatic or steric stabilization. Thus, this thorough particle size and charge analysis is a tool for quick detection of broad particle distributions or aggregates. © 2000 Wiley-Liss, Inc. and the American Pharmaceutical Association J Pharm Sci 89: 1317–1324, 2000

Keywords: iron oxide particles; magnetic resonance imaging; photon correlation spectroscopy; zeta potential; aggregation

INTRODUCTION

Superparamagnetic iron oxide particles (SPIO) stabilized by polysaccharides are important organ-specific contrast media in magnetic resonance imaging (MRI).[1] The size and surface properties of the particles determine their biological and pharmacological properties (e.g., blood half-live and tissue distribution). The diagnostic potential of SPIO in the detection of small liver and spleen metastases is well established,[2–6] but to make new indications accessible (e.g., their application in magnetic resonance (MR) lymphography), rapid uptake by the liver and spleen has to be prevented.[7]

One approach to slowing down "first-pass" elimination in the dominant organs (i.e., liver and spleen) of the mononuclear phagocyte system (MPS) and to enabling extravasation is to reduce the hydrodynamic sizes of the particles.[8–10] Even small differences in the overall size (e.g., 60 versus 30 nm) allow differentiation between a "liver-specific" and a "lymphotropic" SPIO because the consequence for the biological fate, and thus the diagnostic value, is obvious from MR images: only the 30-nm particles are enriched in the lymphatic tissue, whereas the 60-nm particles do not affect signal behavior within the lymph nodes.

Current address: Schering AG, D-13342 Berlin, Germany
Correspondence to: M. Kresse (Telephone: 49-30-46811579; Fax: 49-30-46812168; E-mail: mayk.kresse@schering.de)

Journal of Pharmaceutical Sciences, Vol. 89, 1317–1324 (2000)

To rationally design SPIO contrast agents with respect to their physical properties, in particular their overall size, a sensitive method for determination of particle sizes is essential. As regards state of the art techniques for particle sizing, only photon correlation spectroscopy (PCS) seems to be able to detect iron oxide particles around 20–50 nm with sufficient resolution and accuracy. However, not only the mean size is of interest but also the presence of larger particles resulting from subfractions. Furthermore, the stability (e.g., the tendency to form aggregates) is also of high interest with regard to the storage stability of the commercialized diagnostics.

The aim of this study was therefore to elaborate a sensitive PCS protocol that provides information not only on the mean particle diameter but also on the presence of even small amounts of aggregates, preferentially giving a quantitative measure for the fraction of large particles. Using PCS for the analysis of particle sizes, there are two parameters that can be varied to enhance the resolution of particle size distribution and to detect larger particles (aggregates). One parameter is variation of the delay time, the so-called two-time window analysis.[11] The delay time is defined as the time between two moments at which the intensity of scattered light (decisive parameter for particle size calculation) is measured. The second parameter is changing the measuring angle, which is called multiangle analysis.[12] With these parameters, the degree of aggregates should be detected in quantitative terms.

The highly sensitive detection of aggregates is also a tool for early identification of unstable formulations in a long-term stability test. The stability of iron oxide dispersions strongly depends on the type and quantity of the polysaccharides surrounding the iron oxide core.[13] Aggregation is prevented not only by electrostatic repulsion but also by steric effects due to the polysaccharides present in the medium. Therefore, the second aim of this study was to detect the degree of electrostatic repulsion in the dispersions quantified as zeta potential and to examine whether the iron oxides were stabilized for the most part electrostatically or sterically.

EXPERIMENTAL SECTION

Materials

Iron oxide dispersion A was synthesized using a slightly modified procedure originally described by Hasegawa et al.[14] In particular, iron-II and iron-III precursors were weighed into a round flask in a magnetite-like stoichiometric ratio of 1:2 together with a 10-fold excess of alkali-treated low-molecular-weight dextran (ATD). Precipitation of the iron oxide was initiated by the rapid addition of soda lye. After neutralization, most of the stabilizer was removed by dialysis (Visking tubing, Fluka, Germany) until a 1:1 iron-to-dextran weight ratio was reached. The iron content was 1 mol/L determined by atomic emission spectroscopy (Fisons, UK). Using the anthron method as described elsewhere,[15] the content of the stabilizing polysaccharide was determined to be 56.8 mg/mL.

For batch B, the same procedure was performed in a slightly modified fashion to reduce the particle diameter of the particles. These smaller particles are the result of very fast addition of concentrated soda lye. All other parameters are comparable.

To obtain batch C, ATD of batch B was desorbed by ultrafiltration. Low-molecular-weight dextran solution was added to batch C to produce batch D.

Batch E was synthesized by the IDF.[16] In principle, the synthesis of the CSA-coated particles is comparable to that of the ATD particles. In detail, a better performance of the mixing device and a higher mixing speed is necessary because of the higher viscosity of the starting solution (higher molecular weight of CSA compared with low molecular weight ATD). Furthermore, the purification steps are different because the requirements have to be adjusted because of the higher molecular weight, (e.g., the pore size of the membranes during ultrafiltration; removal of excess stabilizer).

Highly purified water was obtained from the MilliQ plus system (Millipore, Eschborn, Germany), and exceeded all standards for purity (e.g., American Chemical Society).

Methods

Particle size measurements were performed by PCS (Zetasizer 4, Malvern Instruments, Malvern, UK). This method is based on laser light that is scattered by particles. The intensity of scattered light is measured in periods selected by the user and depends on the particle size. Small particles are influenced more by Brownian molecular motion of the water molecules in the dispersion medium, thus diffusing faster than larger ones. This

phenomenon causes differences in the interference of the laser light scattered from differently sized particles; that is, differences in the velocity of intensity fluctuations. Small particles therefore show larger fluctuations around an average scattered light intensity than larger particles (cf. Figure 1).

A correlation function $g(\tau)$ is calculated on the basis of the time-dependent fluctuations of scattered light intensity (cf. eq 1):

$$g(\tau) = e^{-2DK^2\tau} \quad (1)$$

τ: delay time

D: coefficient of diffusion

K: amount of scattered light vector

where τ is the delay time, D is the coefficient of diffusion, and K is the amount of scattered light vector. The parameter K can be calculated according to:

$$K = \frac{4\pi n}{\lambda} \sin\left(\frac{\theta}{2}\right) \quad (2)$$

n: refraction index of suspension medium

λ: laser wave length

θ: angle of scattered light

where n is the refraction index of the suspension medium, λ is the laser wavelength, and θ is the angle of scattered light. The diffusion coefficient is accessible with these data, and the mean diameter can be calculated by applying the Einstein equation. The difference between this calculated correlation function $g(\tau)$ and the theoretical correlation function of monomodal particles that display this average diameter yields information about particle size distribution, which is expressed as the polydispersity index (PI). For detailed information see Müller and Schuhmann.[17] The correlation function, and therefore the resulting particle diameter, can be influenced by varying two parameters as described next.

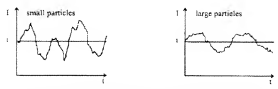

Figure 1. Small and large particles: comparison of time-dependent fluctuations in the intensity of scattered light (I) around an average intensity (i) (based on ref 11).

Multiangle Analysis

At small angles, large particles display increased laser light scattering.[17] Thus, these particles have more weight in particle size calculations than small particles when calculating the intensity-weighted PCS average diameter. No significant angle dependence is detectable in the scattered light intensity of very small particles ($<\lambda/10$; cf. Figure 2). Though particles in the range of $\lambda/10$ were under investigation, multiangle analysis was used to detect larger particles (e.g., aggregates possibly present in the dispersions, which have heavier weighting at small angles). The larger the particles are or the higher the number of the large particles is, the higher are their intensity distribution and the calculated PCS diameter at low scattering angles.

Two-Time Window Analysis

The calculated particle diameter depends on the delay time, which is the period between two moments of scattered light registration. In a very short delay time (only a few microseconds), only small particles show a pronounced decay in the correlation function; the slow intensity fluctuations of the large particles affect little the decay of the function. This phenomenon is reversed when using high delay times. The decay of the function

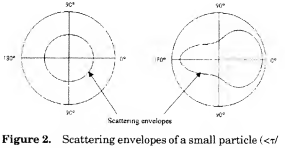

Figure 2. Scattering envelopes of a small particle ($<\tau/10$, left) and a distinctly large particle (right). The intensity contribution of the large particle to the total detected intensity is higher, therefore the intensity mean diameter is higher at low angles.

is mainly affected by the large particles, whereas the contribution of the small ones is limited to the first few channels of the correlation function. Increasing the delay time leads to heavier weighting of larger particles.

Zeta Potential Analysis

The zeta potential was determined by laser Doppler anemometry. Using this method, the particle charge is determined from the particle velocity in an electric field. The particle velocity can be calculated from changes in the frequency of laser light scattered by the particles.

Of course, the particle velocity depends on the strength of the electric field. Because of this dependence, the concept of electrophoretic mobility is commonly used in calculating the zeta potential. Electrophoretic mobility (μ_E) is defined as follows:

$$\mu_E = \frac{v}{E} \tag{3}$$

v: - particle velocity (cm/s)

E: - field strength (esu V/cm)

where v is the particle velocity (cm/s) and E is the field strength (esu V/cm). The laser beam is scattered by these moving particles and shows frequency changes due to the Doppler effect. The extent of the frequency change depends on the particle velocity. Therefore, the particle velocity can be calculated from the frequency movement:

$$f_d = \frac{2 \sin(\theta/2) v}{\lambda} \tag{4}$$

f_c - Doppler frequency

$\theta/2$ - detection angle of scattered light

λ - wavelength of the laser light

v - particle velocity

where f_d is the Doppler frequency, $\theta/2$ is the detection angle of scattered light, λ is the wavelength of the laser light, and v is the particle velocity.

Using the values of particle velocity obtained from eq 4, the electrophoretic mobility can now be calculated (eq 3).

The calculation of the zeta potential ζ from the electrophoretic mobility was done according to the Helmholtz–Smoluchowski formula:[18]

$$\zeta = \frac{4\pi\eta\mu_E}{\varepsilon} \tag{5}$$

μ_E: – electrophoretic mobility

η: – viscosity

ε: – dielectric constant

where μ_E is the electrophoretic mobility, ε is the viscosity, and ε is the dielectric constant.

Taking standard laboratory conditions into consideration and using SI units, the zeta potential ζ can be calculated from the electrophoretic mobility μ_E as follows:

$$\zeta = 12.85\mu_E \quad [(\mu m/s)/(V/cm)] \tag{6}$$

More detailed information about calculation of the zeta potential is given in Müller.[19]

Zeta potential measurements were performed in MilliQ water (conductivity ~5 μS) with a pH in the range 5.0–5.5. The zeta potential is affected in a minor way by small pH changes within this range.[13] The other medium used for zeta potential measurements was the original dispersion medium. The original medium was a solution of polysaccharides with the same concentration as was present in the corresponding iron oxide batch (Zetasizer 4, Malvern Instruments, Malvern, UK).

RESULTS AND DISCUSSION

Particle Size Characterization

The iron oxide dispersions investigated are characterized in Table 1. Firstly, the mean diameter of the particles was detected at an angle of 90° using a delay time of 5 μs. This delay time represents detection of the main population in the expected particle size range ~ 20–50 nm. At lower angles, larger particles show a greater intensity of scattered light.[17,20] Therefore, these larger particles

Table 1. Chemical Composition Potential Application of the Batches for MRI

Dispersion	[Fe] in % [w/v]	Coat in % [w/v]	Target Tissue
A	5.4	5.6% ATD[a]	Liver
B	5.7	5.2% ATD	Lymph nodes
C	3.3	1.6% ATD	Lymph nodes
D	1.7	0.8% ATD; 19.3% Dx[b]	Lymph nodes
E	1.7	3.3% CSA[c]	Liver

[a] ATD, Alkali-treated dextran (~2–4 kDa).
[b] Dx, low molecular weight dextran (~1 kDa).
[c] CSA, chondroitin-4-sulfate (~40 kDa).

have a heavier weighting when the particle sizes are computed, thus leading to larger particle diameters than the parameters representing the main population (90°, 5 μs). Figure 3 shows the mean particle diameters of the batches (detection angle: 90°) as well as the diameters obtained by measuring at smaller angles (detection angles: 60° and 45°). As already mentioned, contrast agents for lymph node imaging (B, C, D) displayed smaller diameters (~30 nm) than those for liver imaging (A, E: ~60 and 105 nm, respectively). When the diameters of each batch are compared at these three angles, only very small differences are detectable. Thus, the batches seemed to be free of aggregates, and a nearly monomodal particle size distribution was expected using multiangle analysis at a delay time of 5 μs.

Nevertheless, the sensitivity of aggregate detection can be enhanced by increasing the delay time. Larger particles or aggregates show smaller fluctuations in the intensity of scattered light compared with smaller particles (cf., Figure 1). These smaller fluctuations are hardly detected when the delay time is very short (e.g., 5 μs). The contribution of the larger particles to the measured fluctuations in light intensity increases with longer delay times. Thus, the resulting particle size increases. This effect, again shown at three angles, can be seen in Figure 4. For the batches containing small particles of ~30 nm (B, C, D), the delay time was increased to as much as 50 μs, whereas for A and E it was 100 μs.

When the particle sizes of each batch are compared at the usually applied measuring angle of 90°, it can be seen that there was no marked difference in particle size for B and E. The size is similar applying a short delay time of 5 μs (cf. Figure 3) or a longer delay time of 50–100 μs (cf., Figure 4). This similarity indicates the absence of aggregates. On the contrary, the particle size increased at increased delay time in the case of batches A, C, and D. The differences amounted to ~ 7 nm (A), 9 nm (C), and even 20 nm (D; detection angle 90°).

Because of the increased scattered light intensity of larger particles at 45°, larger mean dia-

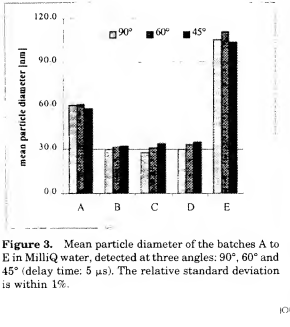

Figure 3. Mean particle diameter of the batches A to E in MilliQ water, detected at three angles: 90°, 60° and 45° (delay time: 5 μs). The relative standard deviation is within 1%.

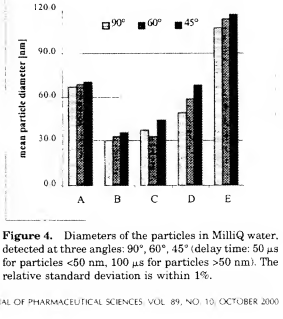

Figure 4. Diameters of the particles in MilliQ water, detected at three angles: 90°, 60°, 45° (delay time: 50 μs for particles <50 nm, 100 μs for particles >50 nm). The relative standard deviation is within 1%.

meters were detected at 45° than at a detection angle of 90°. These differences were within a range of ~3 nm (A) to ~9 nm (E), except for batch D with a difference of ~ 20 nm (Figure 4, long delay time 50 μs). From this, D could be classified as the batch containing most aggregates and the widest particle size distribution. However, the size differences were relatively low for the other batches, and the measuring parameters were therefore optimized further.

Multiangle analysis and two-time window analysis were combined to enlarge the detectable differences between the batches and to quantify the extent of aggregation. The mean diameter of the particles (90°, 5 μs) was subtracted from the diameters obtained with measuring parameters using heavier weighting of larger particles (45°, 50 or 100 μs). Consequently, a particle size difference Δd correlating to the extent of aggregates in the batches was yielded (cf., Figure 5). As expected, batch D showed clearly the largest size difference Δd (~39 nm). Batch B showed the lowest amount (~5 nm), and the difference of C (~10 nm), E (~nm), and D (~16 nm) were in a comparable range. It has to be remembered that the particle diameter of the batches varies from 30 to 105 nm. Therefore, these differences Δd have to be related to the particle size of the batch to which they belong, as shown in Figure 6.

The most stable iron oxide dispersion was batch E, with a Δd of ~11% when this sensitive method is employed for the detection of aggregates. Batches A and B were stable, as is shown well by the slightly increased values for Δd

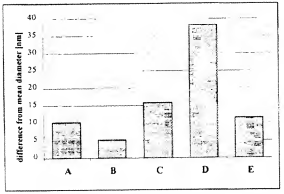

Figure 5. Subtraction of the mean particle diameter (90°, 5μs) from the diameter measured with special weighting of larger particles or aggregates (45°/50 or 100 μs). The difference Δd is a quantitative measure of the presence of aggregates.

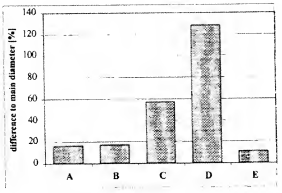

Figure 6. Subtraction of the mean particle diameter (90°, 5μs) from the diameter measured with special weighting of larger particles or aggregates (45°/50 or 100 μs). The difference is shown as percentage points in relation to the mean particle population.

(both~17%). The fraction of aggregates is markedly increased in batch C (~57%) and, in particular, in batch D, recognizable by the Δd of ~128% (cf., Figure 6). This combination of multiangle and two-time window analysis provides an excellent tool to detect and quantify aggregates in particle dispersions that are not accessible to laser diffractometry because of their small particle sizes.

The reasons for the rapid particle growth in C and D can be explained by the production of these batches. Batch C was produced by ultrafiltration of batch B, resulting in a decrease of carboxydextran molecules. It is presumed that the concentration of carboxydextran molecules in this dispersion (1.6%) is insufficient for effective steric stabilization. A reduced particle size — the aim of ultrafiltration of B by thinning out the macromolecular adsorption layer (desorption) — could not be achieved (cf., Figure 2). The addition of uncharged, low-molecular-weight dextran to batch C to obtain batch D should yield an altered particle surface with nearly the same particle diameter being retained. Nevertheless, the secondary effect was a rapid formation of aggregates by bridging effects due to the uncharged dextran molecules. Batches C and D did not seem to be specific contrast agents for MR lymphography because of their wide particle size distribution (formation of aggregates).

Particle Charge Characterization

The extent of aggregates in the iron oxide batches was shown by the particle size characterization

just described; particle charge determination can probably explain the type of stabilization effects. Figure 7 shows the zeta potentials of the batches measured in MilliQ water.

The highest zeta potential was present in batch E particles (zeta potential of −55 mV), followed by batch A (−45 mV). In this range of zeta potential values, particle aggregation is prevented by electrostatic repulsion,[19] as confirmed by particle size measurements. The zeta potentials of B, C, and D were nearly the same (−32 mV), which seems to be in contradiction to their different content of aggregates (cf., Figure 5). Zeta potentials in this range are related to no aggregation or to only little aggregation in the dispersion.[19] The particle growth in C and D was not explainable by charge determination in MilliQ water. Charge determination in MilliQ water yields a zeta potential identical to the Stern potential; that is, it is related to the particle surface charge but not to the thickness of the diffuse layer in the original dispersion medium. Therefore, the zeta potential was determined using the original liquid as the measuring medium (the same concentration of polysaccharides present in each batch (cf. Table 1) was dissolved in MilliQ water). The zeta potentials of batches A– D are shown in Figure 8.

The zeta potentials of batches B and D, ~−2 and −4 mV, respectively, are within a range of strong aggregation. The aggregation tendency for batch B was very small (cf., Figures 5 and 6), steric stabilization being the driving force preventing particle aggregation. The results obtained from determination of the particle charge in the original medium explain the detected instability of batch D. Dispersion D possesses a

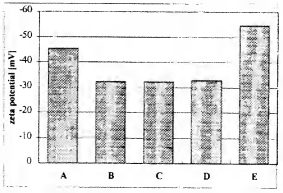

Figure 7. Zeta potentials (mV) of the batches in MilliQ water (n = 6). The standard deviations do not exceed 3 mV.

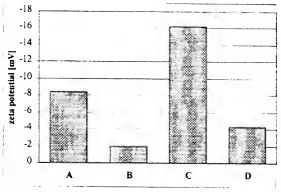

Figure 8. Zeta potentials (mV) of the batches in original medium (solution of polysaccharides with the same concentration as present in each iron oxide batch: n = 6).

higher amount of dissolved molecules (ATD and low-molecular-weight dextran) than batch B, but the majority of these molecules are uncharged dextran molecules. Thus, the high amount of uncharged molecules in batch D is presumed to be responsible for bridging effects leading to particle aggregation.

The zeta potentials of the dispersions A and C, ~−8 and −16 mV, respectively, are in the range of flocculation.[19] The amount of dissolved ATD molecules present in batch A is comparable to that in batch B. Steric stabilization is therefore apparently the reason for low particle aggregation, which is supported by greater electrostatic repulsion than that of dispersion B.

In batch C, elctrostatic stabilization was greatest of all the dispersions analyzed, but particle aggregation cannot be completely avoided (cf., Figures 5 and 6). Particle aggregation is attributable to a deficiency of dissolved ATD molecules (cf., Table 1), thus making steric stabilization less efficient.

CONCLUSION

The particle size distribution of ultrasmall particles (up to 100 nm) can be characterized with a combination of two-time window analysis and multiangle analysis. These methods provide much more precise information about the aggregation tendencies of such dispersions as the PI of PCS measurements at 90° scattered angle.

Additional charge determinations make it

easier to describe the type of stabilization present in the dispersion. Conclusions cannot be drawn about particle stability solely on the basis of charge determination in MilliQ water and in the original medium (e.g., there are no differences detectable between the batches B and D). Only in combination with intensive particle size analysis such as two-time window and multiangle analysis is it possible to characterize particle growth and stabilization effects.

Using two-time window and multiangle analysis in combination with particle charge determination as characterization methods, rapid information on the batch stability is accessible. Therefore, production of ultrasmall particle dispersions can be optimized very early.

REFERENCES

1. Saini, S, Frankel R-D, Stark DD, Ferrucci JT. 1988. Magnetism: A primer and review. Am J Roentgenol 150:735–743.
2. Ferrucci JT. 1986. MR imaging of the liver. Am J Roentgenol 147:1102–1116.
3. Saini S, Stark DD, Hahn PF. 1987. Ferrite particles: A superparamagnetic MR contrast agent for the reticuloendothelial system. Radiology 162: 211–216.
4. Weissleder R, Saini S, Stark DD, Wittenberg J, Ferruci JT. 1988. Dual-contrast MR imaging of liver cancer in rats. Am J Roentgenol 150:561–566.
5. Magin RL, Bacic G, Niesmann MR, Alameda JC, Wright SM, Swartz HM. 1991. Dextran magnetite as a liver contrast agent. Magnet Reson In Med 20:1–16.
6. Saini S, Edelman RR, Sharma P, Li W, Mayo-Smith, W, Slater GJ, Eisenberg PJ, Hahn PF. 1995. Blood-pool MR contrast material for detection and characterization of focal hepatic lesions: initial clinical experience with ultrasmall superparamagnetic iron oxide (AMI-227). Am J Roentgenol 164:1147–1152.
7. Weissleder R, Papisov MI. 1992. Pharmaceutical iron oxides for MR imaging. Rev Magn Reson Med 4:1–20.
8. Wagner S, Pfefferer D, Taupitz M, Kresse M, Lawaczeck R, Hamm B, Wolf K-J. 1992. Intravenous MR-lymphography with ultrasmall iron oxide particles: *In vivo* and *ex vivo* examinations in rats. SMRM; Society of Magnetic Resonance in Medicine - Book of Abstracts, 570.
9. Vassallo P, Matei C, Heston WDW, McLachlan SJ, Koutcher JA, Castellino RA. 1994. AMI-227-enhanced MR lymphography: Usefulness for differentiating reactive from tumor-bearing lymph nodes. Radiology 193:501–506.
10. Anzai Y, Blackwell KE, Hirschowitz SL, Rogers JW, Sato Y, Yuh WTC, Runge VM, Morris MR, McLachlan SJ, Lufkin RB. 1994. Initial clinical experience with dextran-coated superparamagnetic iron oxide for detection of lymph node metastases in patients with head and neck cancer. Radiology 192:709–715.
11. Müller RH, Heinemann S. 1992. Fat emulsions for parenteral nutrition. I: Evaluation of microscopic and laser light scattering methods for the determination of the physical stability. Clin Nutr 11: 223–236.
12. Bott S. 1988. Enhanced resolution particle size distribution by multiple angle photon correlation spectroscopy. In: Lloyd PJ, editor. Particle size analysis. New York: John Wiley Sons Ltd., pp 77–88.
13. Thode K. 1996. Spezifische Kontrastmittel für die Magnetresonanz-Tomographie: Physikochemische Charakterisierung und Studien zur Plasmaproteinadsorption. Ph.D. Thesis, The Free University of Berlin, 1996; pp 103–104.
14. Hasegawa M, Ito Y, Yamada H, Nagae H, Tozawa N, Hino Y, Kito K, Hokukoku S, Lawaczeck R, Ebert W, Pfefferer D, Wagner S, Kresse M. 1992. Water-soluble carboxypolysaccharide-magnetic iron oxide complex of small particle size. Patent WO 94/03501.
15. Kresse M. 1994. Spezifische Kontrastmittel für die Magnetresonanz-Tomographie: Herstellung und Charakterisierung von superparamagnetischen Transferrin Dextran- und Transferrin-Chondroitin-Magnetiten. Ph.D. Thesis, The Free University of Berlin, pp 34–35.
16. Pfefferer D. 1993. Synthese, in-vitro und in-vivo-Charakterisierung von Chondroitin-4-sulfat-stabilisierten superparamagnetischen Eisenoxiden und ihre Anwendung als Kontrastmittel für die Magnetische – Resonanz – Tomographie. Ph.D. Thesis, The Free University of Berlin, p 13.
17. Müller RH, Schuhmann R. 1996. Teilchengrößenmessung in der Laborpraxis, 1st ed.; Stuttgart: Wissenschaftliche Verlagsgesellschaft.
18. Smoluchowski M. 1921. In: Handbuch der Elektrizität und des Magnetismus, Vol. II. Leipzig.
19. Müller RH. 1996. Zetapotential und Partikelladung in der Laborpraxis, 1st ed.; Stuttgart: Wissenschaftliche Verlagsgesellschaft.
20. Schuhmann R. 1995. Physikalische Stabilität parenteraler Fettemulsionen. Ph.D. Thesis, The Free University of Berlin, p 28.